Sequences of Fracture Toughness Micromechanisms in PP/$CaCO_3$ Nanocomposites

R. Lesan Khosh, R. Bagheri, S. Zokaei

Polymeric Materials Research Group, Department of Materials Science and Engineering, Sharif University of Technology, Tehran 11365-9466, Iran

Received 3 January 2008; accepted 4 July 2008
DOI 10.1002/app.28909
Published online 23 September 2008 in Wiley InterScience (www.interscience.wiley.com).

ABSTRACT: Mechanical properties and fracture toughness micromechanisms of copolypropylene filled with different amount of nanometric $CaCO_3$ (5–15 wt %) were studied. *J*-integral fracture toughness was incorporated to measure the effect of incorporation of nanoparticle into PP matrix. Crack-tip damage zones and fracture surfaces were studied to investigate the effect of nanofiller content on fracture toughness micromechanisms. It was found that nanofiller acted as a nucleating agent and decreased the spherulite size of polypropylene significantly. *J*-integral fracture toughness (J_c) of nanocomposites was improved dramatically. The J_c value increased up to approximately two times that of pure PP at 5 wt % of nano-$CaCO_3$. The fracture micromechanisms varied from rubber particles cavitation and shear yielding in pure PP to simultaneous existence of rubber particles cavitation, shear yielding, filler particles debonding, and crazing in PP/$CaCO_3$ nanocomposites. © 2008 Wiley Periodicals, Inc. J Appl Polym Sci 110: 4040–4048, 2008

Key words: nanocomposites; polymer-matrix composites; fracture toughness; crack

INTRODUCTION

Polypropylene is widely used in automotive industry and household applications, because of its desirable mechanical and physical properties. Thus, there is special attention to PP and its compounds to establish the "monomaterial system" in automotive industries.[1] Consequently, this increasing market demand has triggered extensive studies to further understand the structure-properties relationship and toughening mechanisms of polypropylene. Mechanical properties and dominant fracture toughness micromechanisms of polypropylene depend on various parameters such as crystalline morphology/structure and additives, which incorporated to the matrix. Inorganic fillers such as glass (bead and fiber), talc, mica, and calcium carbonate (micron size) are commonly incorporated into PP matrix to enhance its mechanical and physical properties and also to reduce its cost. Introduction of each of these inorganic fillers may change the crystalline structure and morphology of polypropylene matrix[2–4] as well. Micro-$CaCO_3$ is one of the first fillers used in polypropylene.[5] It is shown that addition of micro-$CaCO_3$ reduces the fracture toughness of PP.[5,6]

In recent years, in addition to traditional modifiers, such as rubber particles[7,8] and micro-size fillers,[5,6] nano size modifiers have been also introduced to improve physical and mechanical properties of PP.[9–16] Among these modifiers, incorporation of organoclay and nanometric $CaCO_3$ has the most attraction. It is reported that addition of nano-$CaCO_3$ improves toughness and stiffness of PP.[9,10,13,17–20] However, just a few studies have been carried out to investigate the effect of nano-$CaCO_3$ particles on fracture toughness micromechanisms of polypropylene.[9,10,13,17–20] Therefore, it is attempted here to elucidate the effect of nanoparticles on mechanical properties and dominant fracture toughness micromechanisms in PP/$CaCO_3$ nanocomposite.

EXPERIMENTAL

Materials

Nanocomposite was prepared from polypropylene copolymer (R40 Arak Petrochemical) with melt flow index of 7 g/10 min (2.16 kg at 190°C) together with SOCAL312 precipitated calcium carbonate (19 m^2/g specific surface) from SOLVAY, with the average size of 70 nm. According to SOLVAY's products data sheet, the calcium carbonate nanoparticles were coated with stearic acid. Nanometric calcium carbonate particles were dried in a vacuum oven at 80°C for 10 h before melt-compounding. Subsequently, polypropylene granules and different amount of

Correspondence to: R. Bagheri (rezabagh@sharif.edu).
Contract grant sponsor: High-Tech Center of the Ministry of Industries and Mines.

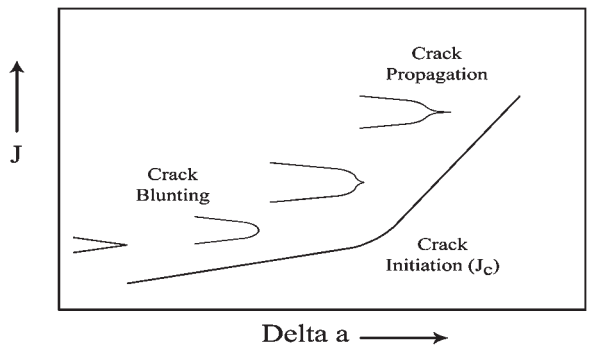

Figure 1 Schematic representation of crack growth at elastic-plastic materials.

nanometric calcium carbonate particles (5, 10, and 15 wt %) were mixed physically in a mixer for 30 min. During this process, nanoparticles were adhered on the PP granules surface electrostatically. Then, each batch were melt blended (in a successive temperature range of 160–120°C) in a corotating twin-screw extruder ($L = 1.2$ m, $D = 53$ mm) and then injection molded using a MonoMat 80 injection molding machine. The barrel temperature profile was set between 210 and 230°C from feed zone to nozzle. The mold temperature was held about 50°C via warm water circulation.

Mechanical properties evaluation

Tensile test

The modulus of elasticity and yield stress of pure PP and the nanocomposites were measured according to ASTM D638. The tests were performed on a universal Hounsfield frame (H10KS) at 5 mm/min crosshead speed. A 100SC extensometer was incorporated to determine modulus of elasticity.

J-integral

Elastic-plastic fracture mechanics (EPFM) principles were applied to evaluate fracture toughness of materials using single-edge notched three-point bending (SEN-3PB) specimens. The multiple specimen technique with 1 mm/min crosshead speed was used to evaluate *J*-integral fracture toughness. Precracks were introduced via pushing a razor blade at the root of notches made by a saw cut. The crack length was 7.7 mm ($a/w = 0.6$) for all specimens. In this technique, the increment of the diameter of the stress whitened-zone at the crack-tip is used in place of the crack length increment.[21] To measure the damage zone lengths, the side surface of specimen was polished down to half of the thickness of samples by silica paper grounding and subsequently 0.05 μm alumina particles polishing. The length of damage zone, i.e., crack extension and length of crack-tip deformation zone, was measured by reflective optical microscopy in dark-field mode. *J*-values were calculated based on ASTM D6068. In this procedure, as will be seen, *J*-Δ*a* measured did not follow a conventional *R*-curve behavior. The values measured lie on two intersected lines with different slopes and the intersection point is considered the critical *J*-integral value or J_c.[21] The J-Δ*a* curve is schematically shown in Figure 1. As shown in Figure 1, the J-Δ*a* slope increases sharply as the crack initiates.

Microscopy

Transmission optical microscopy

The size of PP spherulite and dominant fracture toughness micromechanisms were studied using transmission optical microscopy (TOM) in bright field and cross-polarized modes, using samples polished down to about 100 μm thick. Double-edge notched four-point bending test (DEN-4PB) with crosshead speed of 1 mm/min was applied to investigate crack-tip damage zone micromechanisms (Fig. 2).[22] The DEN-4PB damage zone of the subcritically propagated crack was cut along crack growth direction, but perpendicular to fracture surface, using a diamond saw and subsequent polishing. The thin sample containing the damage zone was studied by Olympus EMP3 optical microscope.

Scanning electron microscopy

A JEOL JXA 840 scanning electron microscope (SEM) was incorporated to investigate the fractured surfaces of the pure PP and nanocomposite. All SEM specimens were given a coat of gold to avoid charge build up and thereby improve the image quality.

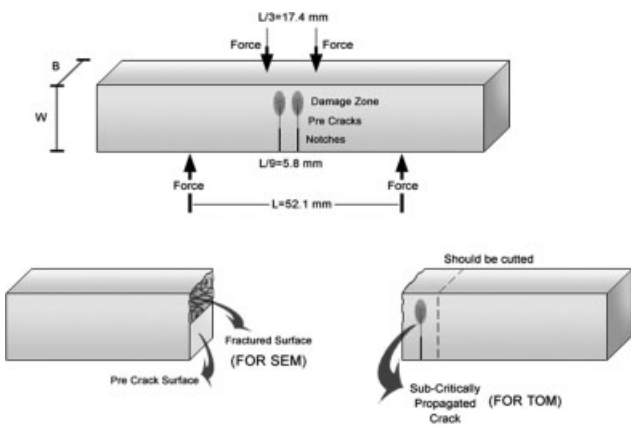

Figure 2 Four-point bending specimens for transmitted optical and scanning electron microscopy.

Transmission electron microscopy

To examine the dispersion of nanometric calcium carbonate particles in the matrix, transmission electron microscopy (TEM) was utilized. TEM, specimens were first trimmed to the size of 1 mm × 1 mm × 5 mm. The trimmed blocks were then stained in Osmium Tetraoxide (OsO_4) for about 3 days. The stained blocks were embedded into low-viscosity epoxy resin before ultrathin (70 nm thick) slices were cut. Ultramicrotomy was conducted using a Reichert-Jung Ultracut-E® equipped with a Diatome® 45° diamond knife. TEM observation was performed on a PHILIPS CM 200 STEM operated at 200 kV.

Physical properties evaluating

Differential scanning calorimetry

Crystallization behavior of pure polypropylene and PP/$CaCO_3$ nanocomposites were studied using a TA Instrument (Q100) differential scanning calorimeter (DSC). About 3–10 mg of each sample was heated up from 25 to 200°C at a heating rate of 10°C/min. The sample was then held for 5 min at 200°C to eliminate thermal history of the sample, induced during injection molding process, before being cooled to room temperature.

Subsequently, a second heating cycle was conducted to measure the enthalpy of fusion. The degree of crystallinity of the samples was calculated from the ratio of measured enthalpy to the enthalpy value for 100% crystalline PP, taken as 209 J/g.[23]

RESULTS AND DISCUSSION

Morphological study

TEM micrograph of ultramicrotome section of PP/10 wt % nano-$CaCO_3$ (PP/10 wt % *n*-CC) is illustrated in Figure 3. This figure confirms the appropriate dispersion of particles in the matrix. Figure 4 compares TOM micrographs of pure PP with PP/5 wt % $CaCO_3$ nanocomposite. As seen, by adding the nanofiller, the spherulite size is reduced significantly. In fact, the spherulitic structure has been almost disappeared. According to DSC results (Table I), Although addition of nanofiller increases the crystallization temperature of polypropylene, it does not make any change to the degree of crystallinity of

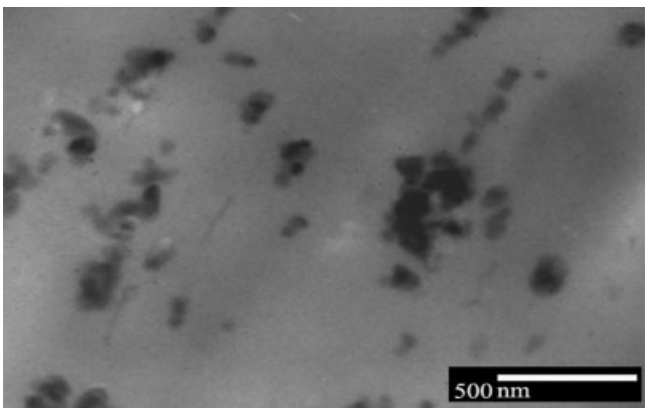

Figure 3 TEM micrograph of PP/10 wt % $CaCO_3$.

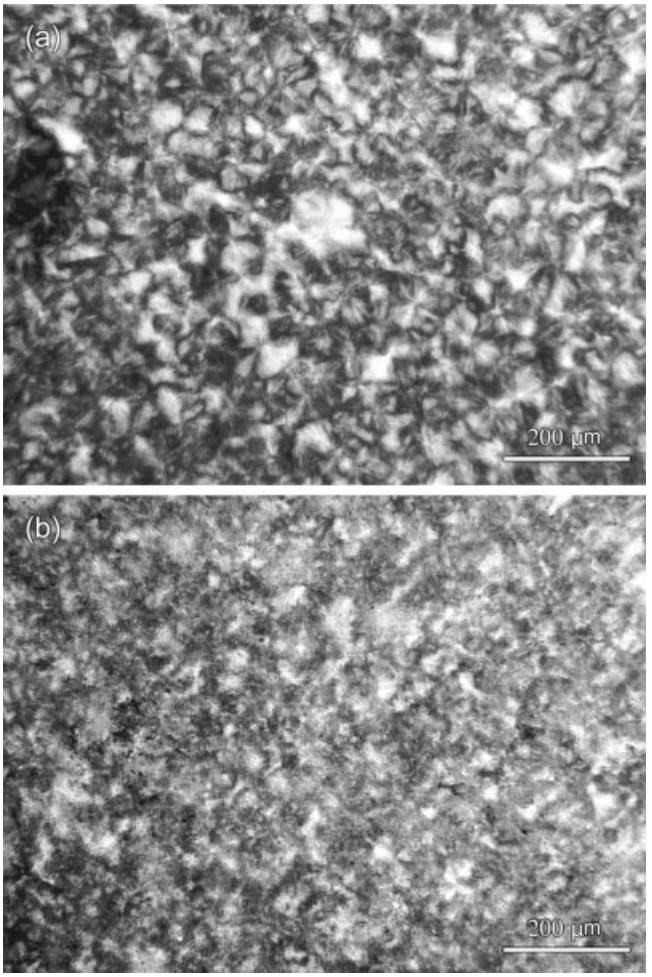

Figure 4 Transmitted optical microscopy under cross-polarized condition shows spherulitic structure of (a) pure PP and (b) PP/5 wt % $CaCO_3$ nanocomposite.

TABLE I
DSC Results of Pure Polypropylene and PP/$CaCO_3$ Nanocomposites

Materials	Crystallization temperature (°C)	Degree of crystallinity (%)
Pure PP	114	23.8
PP/5 wt % *n*-CC	120.5	23.5
PP/10 wt % *n*-CC	123	23
PP/15 wt % *n*-CC	125.5	23

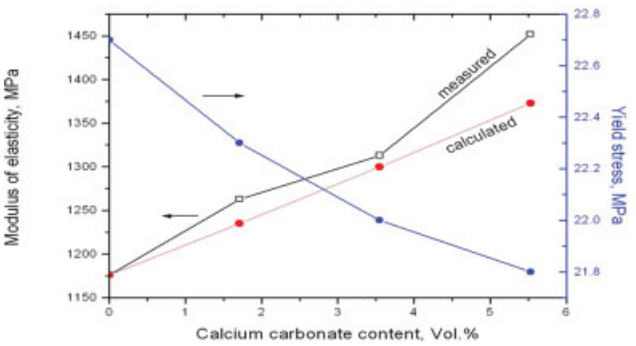

Figure 5 Mechanical properties of pure PP and PP/$CaCO_3$ nanocomposites. [Color figure can be viewed in the online issue, which is available at www.interscience.wiley.com.]

polypropylene. Therefore, it can be stated that nano-$CaCO_3$ particles act as a nucleating agent and destroy the spherulitic structure of the polypropylene matrix.

Mechanical properties of PP/$CaCO_3$ nanocomposites

Tensile properties of pure PP and PP/$CaCO_3$ nanocomposites have been illustrated in Figure 5. Also, calculated modulus of nanocomposites has been shown in this figure. The calculation has been done according to the following equation:

$$E_c = \frac{E_p E_f}{E_p \Phi_f + E_f \Phi_p} \quad (1)$$

where E_c, E_p, and E_f are modulus of nanocomposite, matrix, and filler, respectively, Φ_p and Φ_f are the volume fraction of matrix and nanoparticles, respectively. As seen, while addition of $CaCO_3$ increases the modulus of elasticity, it slightly decreases the yield stress. Similar finding has been observed in microcomposites.[6] For interpretation of this behavior two counter balance effects should be considered, the nucleating and the reinforcing effects of nano-$CaCO_3$. It has been shown, in Figure 4, that the spherulitic structure of nanocomposites has been disappeared, because of nucleating effect of nanoparticle. It has been reported that a decrease in spherulite size decreases the modulus and yield stress of the polymer.[9] As indicated earlier, the degree of crystallinity of all pure and nanocomposite samples are the same. However, reinforcing effect of the nanofiller introduces an increment in the modulus of nanocomposite. Comparing the experimental and calculated modulus (Fig. 5), it can be seen that the increase of the modulus is higher than that of the prediction. The reason for this observation is attributed to the point that the $CaCO_3$ particles have enough adhesion to the matrix in early stages of loading, and thus increase the modulus of elasticity. At higher loading levels, close to the yielding point, however, the debonding occurs that causes a drop in yield stress of the material. The fine spherulitic structure also intensifies this yield stress reduction. However, the reduction of yield stress is not significant.

Effect of nanometric $CaCO_3$ on fracture toughness micromechanisms of polypropylene

J-Δ*a* curves and normalized J_c values for different amounts of filler loading in PP matrix are shown in Figure 6. As seen, all nanocomposites have higher fracture toughness than pure PP. Also, it is noticeable that by adding 5 wt % calcium carbonate into PP, J_c increases dramatically. However, J_c decreases as filler content is further increased. Figure 7 illustrates SEM micrographs of fracture surfaces of pure PP and nanocomposites. Looking at Figure 7, it is evident that addition of 5 wt % nano-$CaCO_3$ to PP intensifies interparticle shear yielding and matrix fibrillation [compare Fig. 7(a,b)]. Further increase of

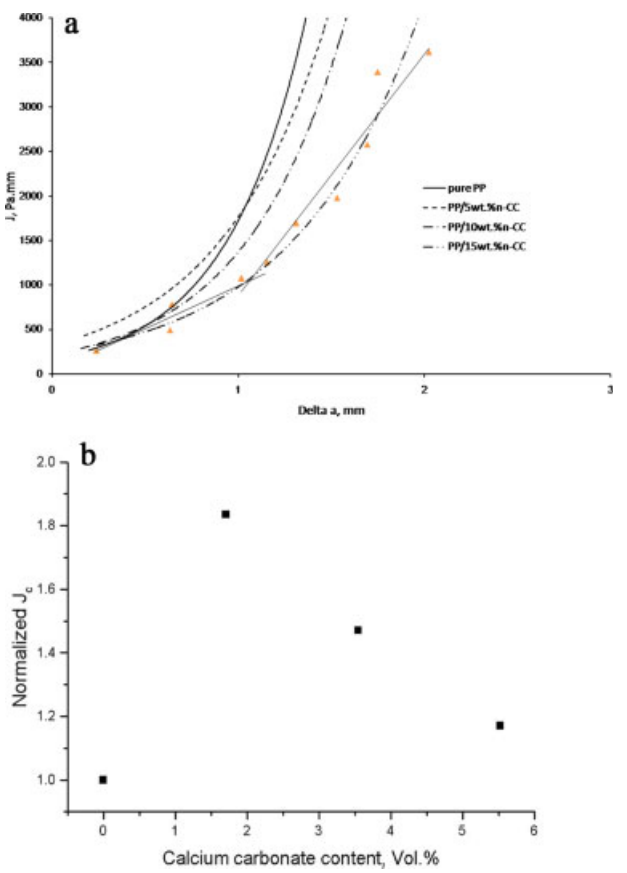

Figure 6 Representation of (a) *J*-Δ*a* curves and b) normalized J_c versus $CaCO_3$ content in PP/$CaCO_3$ nanocomposites. [Color figure can be viewed in the online issue, which is available at www.interscience.wiley.com.]

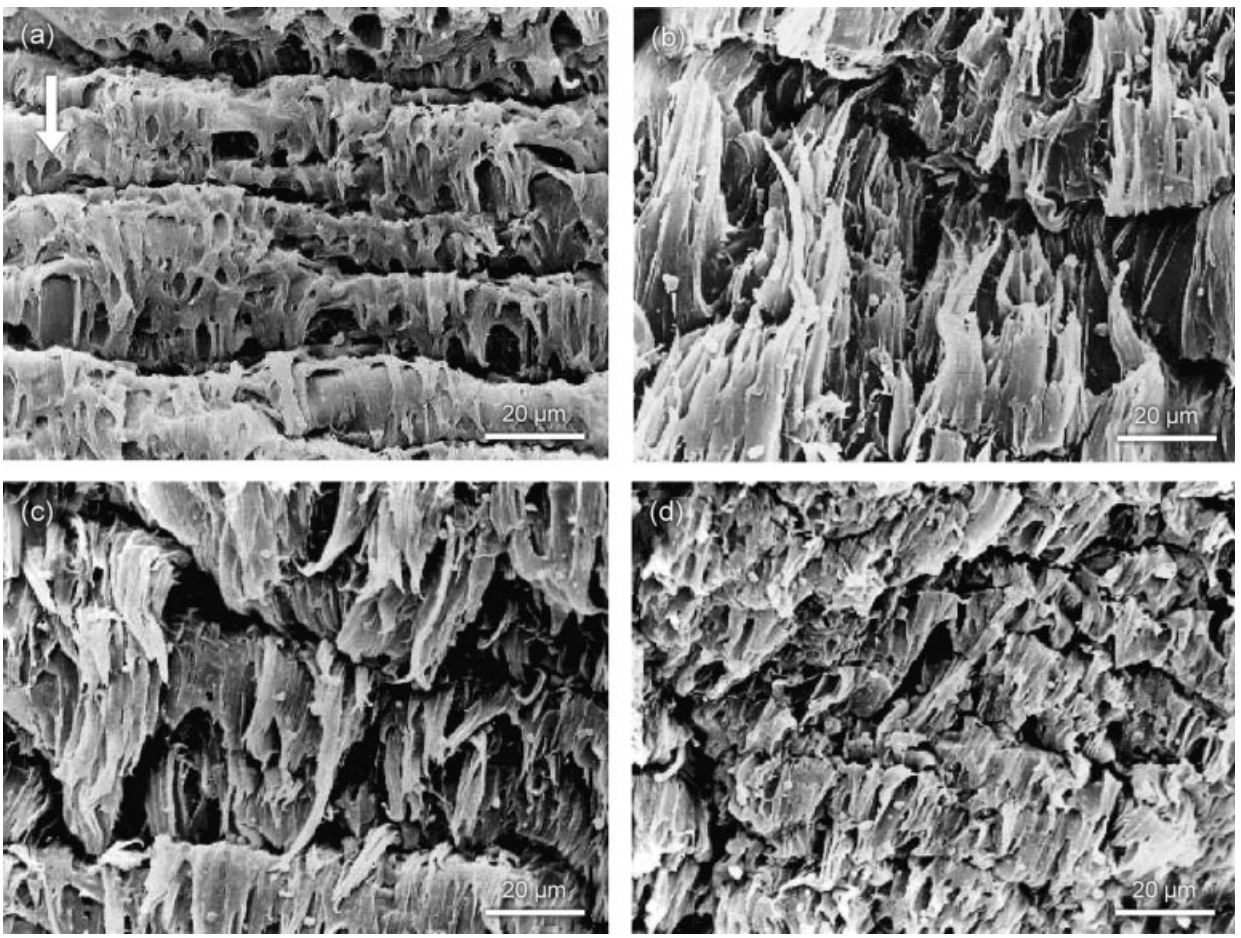

Figure 7 Scanning electron micrographs from fracture surface of (a) pure PP and PP/$CaCO_3$ nanocomposites containing (b) 5, (c) 10, and (d) 15 wt %. Note that the arrow indicates the crack growth direction.

$CaCO_3$, however, results in decreased plastic flow of the interparticle matrix [compare Fig. 7(c,d) with 7(b)]. This observation agrees with that of J_c measurements shown in Figure 7. Figure 8 illustrates transmitted optical microscopy results of the crack-tip damage zones of different materials under bright field and cross-polarized light conditions. In the case of pure PP, as seen in Figure 8(a,b), the dominant fracture toughness micromechanism is cavitation of rubbery particles followed by shear yielding. Note that dark features in Figure 8(a) are due to cavitation of rubber particles at the crack-tip damage zone. In addition, birefringence under cross-polarized condition [Fig. 8(b)] is an indication of shear yielding at the crack-tip.

By adding 5 wt % nano-$CaCO_3$ into polypropylene, similar to pure PP, both cavitation [dark features in Fig. 8(c)] and shear yielding [birefringence in Fig. 8(d)] are the dominant fracture toughness micromechanisms. However, it can be clearly seen that the addition of 5 wt % $CaCO_3$ intensifies shear yielding of the matrix at the crack-tip [note the higher level of birefringence in Fig. 8(d) than that of Fig. 8(b)]. This behavior may be due to two reasons:

1. The debonding of $CaCO_3$ particulates,[10] which trigger the intense shear yielding via triaxial stress relief within the ligaments around the particles (transition of stress state from triaxial to uniaxial or biaxial),[24] and
2. the reduction of spherulite size, which promotes the plastic flow of the matrix.

The induced shear yielding (fibrillation) is also observable on fracture surface in Figure 7(b).

According to fracture toughness measurements, J_c value, energy consumption at the crack-tip damage zone of PP/10 and 15 wt % *n*-CC is lower than that of PP/5 wt % *n*-CC. It may be due to the higher concentration of nanoparticles, which causes aggregation in the matrix. The agglomerated nanoparticles behave like microsize particle and can reduce the fracture toughness of the composite.[6] Therefore, the agglomeration of the particles is an effective phenomenon, which should be considered in this assessment. According to TEM micrograph in Figure 3, there is not any agglomeration of particles. To disprove the appearance of the aggregation of the nanoparticles, the yield stress

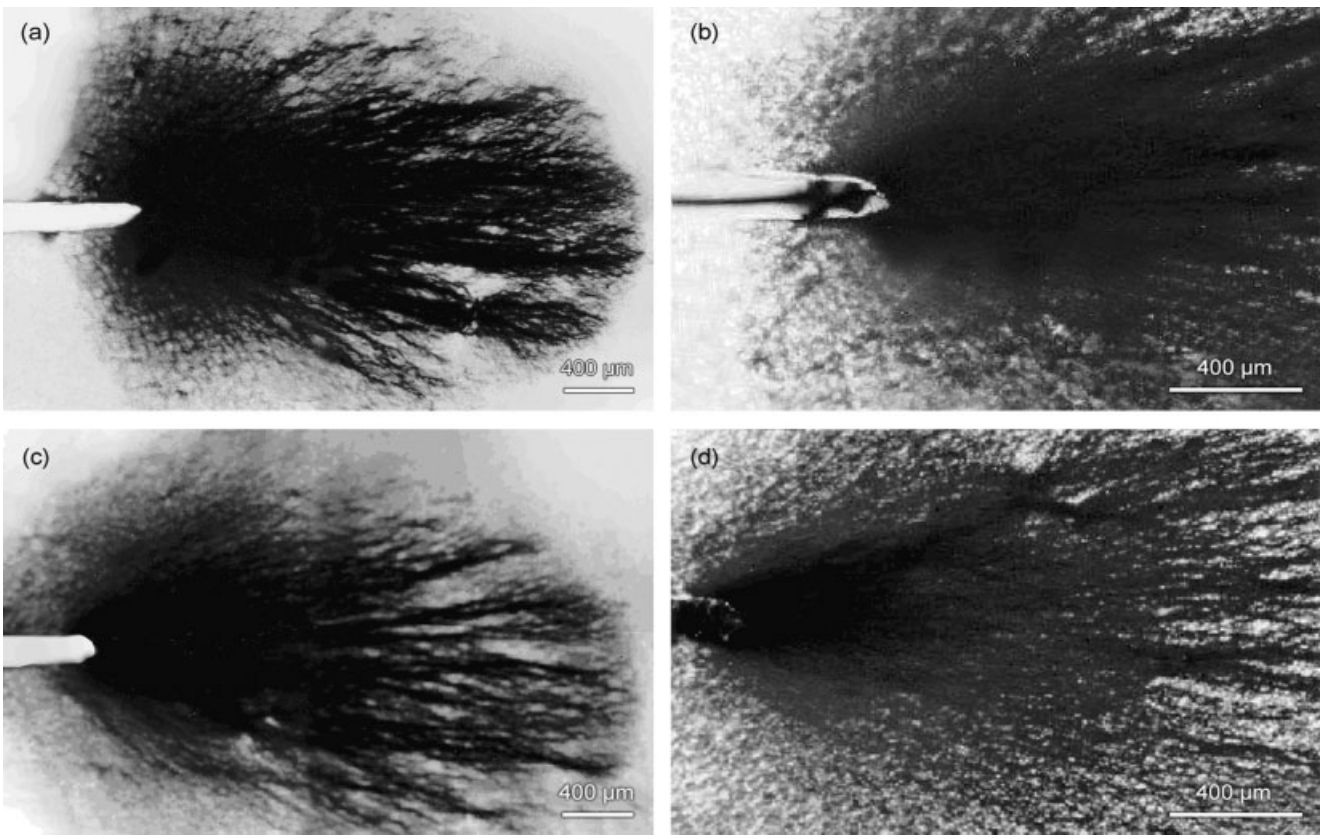

Figure 8 Transmitted optical microscopy form crack-tip damage zone of (a) and (b) pure PP and (c) and (d) PP/5 wt % $CaCO_3$. Note that (a) and (c) micrographs are taken under bright field and (b) and (d) micrographs are taken under cross-polarized light condition.

model in particulate filled composite has been applied[25,26]:

$$\sigma_{\text{yrel}} = \frac{\sigma_y}{\sigma_{y0}} \frac{1 + 2.5\Phi}{1 - \Phi} = \exp(B\Phi) \tag{2}$$

where σ_{yrel}, σ_y, and σ_{y0} are relative yield stress, yield stress of the composite and matrix, respectively, Φ is the volume fraction of the nanofiller and B is a parameter related to the load-bearing capacity of the filler. According to above equation, ln (σ_{yrel}) has linear relationship with volume fraction of filler with a constant slope of B. However, the agglomeration reduces the contact area between the particles and the matrix; so as a result, the value of B should also decrease. In fact, any deviation form straight line indicates the presence of agglomeration.[26] Figure 9 illustrates the relationship between ln (σ_{yrel}) and volume fraction of nano-$CaCO_3$. As seen, there is not any deviation from linearity, which indicates absence of the agglomeration of the filler in all of the nanocomposites. Consequently, the changes in fracture toughness micromechanisms, introduced by higher concentration of nanoparticles, should be responsible for the restriction of plastic flow of the matrix in PP/10 and 15 wt % $CaCO_3$ nanocomposites in comparison with PP/5 wt % *n*-CC.

Because there is similarity in fracture toughness features for PP/10 wt % *n*-CC and PP/15 wt % *n*-CC, only the fracture toughness micromechanisms of PP containing 15 wt % nano-$CaCO_3$ will be studied.

In the case of PP nanocomposite containing 15 wt % calcium carbonate, as seen in Figure 10(a,b),

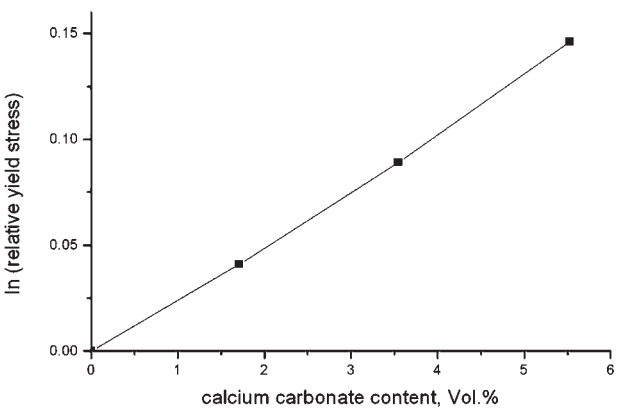

Figure 9 Relationship between ln (σ_{yrel}) and volume fraction of *n*-CC.

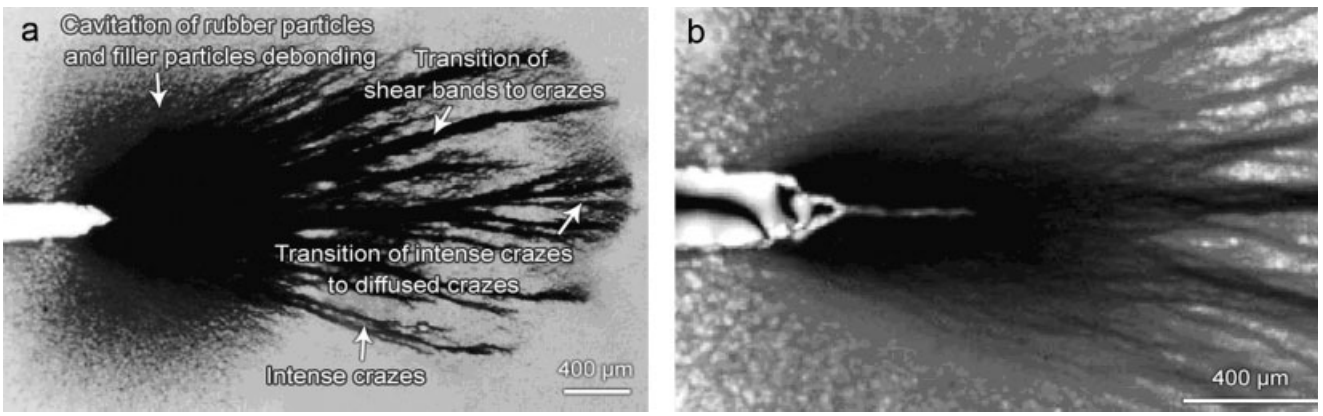

Figure 10 Transmitted optical microscopy form crack-tip damage zone of PP/15 wt % $CaCO_3$.nanocomposite at (a) bright field and (b) cross-polarized conditions.

cavitation of rubber particles, filler particles debonding, shear yielding, and intense and diffused crazing are the active fracture toughness micromechanisms. Transformation of intense shear bands to crazes is distinguishable at the end of the cavitation zone [Fig. 10(a)]. Inverse of such transformation has been reported and discussed by Sue and Wei in PP/SEP system, in which, intense crazing transforms into shear yielding micromechanism.[27] It is believed that the transformation of shear band into crazing is due to the repeated cavitation and debonding, which causes a dilatational shear band or craze-like feature. Similar micromechanism has been reported by Zebarjad et al. in PP/EPR/$CaCO_3$ system.[28] In this case, when the repeated cavitations and microvoids occur in a row, it can act as an initiation of the crazing. Therefore, for the samples with higher concentration of nanoparticles, the formation probability of these crazes is high. This transformation makes the smaller cavitation zone and consequently lower degree of shear yielding (plastic flow). Obviously, intense crazing is less energy consumer in comparison with shear yielding.

At the end of the crack-tip damage zone, the conversion of intense crazes to diffused crazes is also recognizable [Figs. 10(a), 11(a,b)]. The cross-polarized micrograph [Fig. 11(b)] confirms that the dark features seen in Figure 11(a) are intense and diffused crazes (because of the lack of birefringence). As shown in Figure 11(b) by arrows, the intense dark lines are rotating toward mode I as they propagate (considering force lines perpendicular to crack surface). This observation also confirms that the dark features seen are intense crazes, because presence of free surfaces like craze or crack can behave like this manner. Therefore, in general, cavitation, debonding, shear yielding, intense crazing (or craze-like), and finally diffused crazing are the dominant fracture micromechanisms in PP/10 and 15 wt % $CaCO_3$ nanocomposites. The sequences of fracture toughness micromechanisms of pure PP and PP/$CaCO_3$ nanocomposites have been summarized and shown schematically in Figure 12.

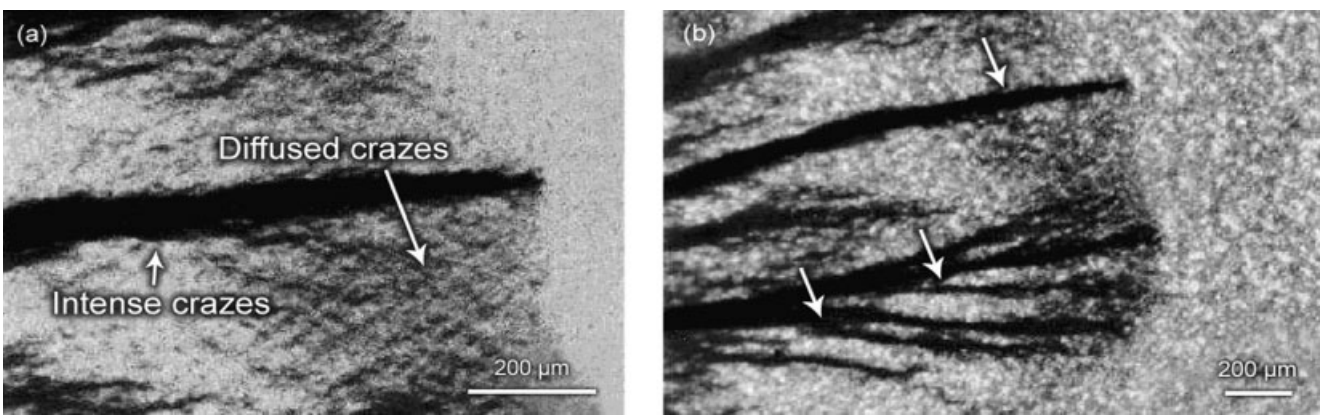

Figure 11 Transmitted optical micrograph of PP/15 wt % $CaCO_3$ nanocomposite at the end of crack-tip damage zone taken under (a) bright field and (b) cross-polarized light condition. The arrows in (b) illustrate the tendency of intense crazes to rotate to mode I.

Materials	Fracture toughness micromechanisms	Scheme
pure co-PP	Rubber particle cavitation and subsequent shear yielding of the matrix	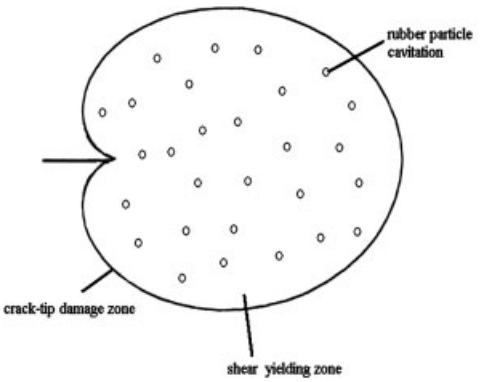
PP/5wt.%n-CC	Rubber particle cavitation/ debonding of $CaCO_3$ particles and subsequent intense shear yielding of the matrix (fibrillation of the matrix)	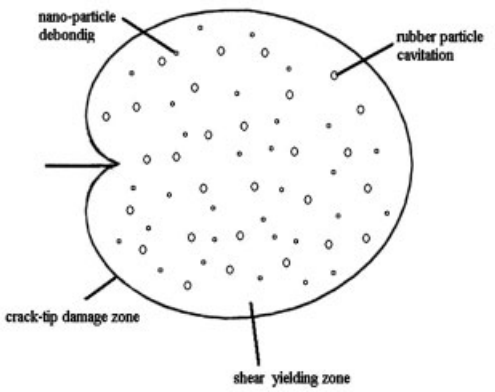
PP/15wt.%n-CC	Rubber particle cavitation/ debonding of $CaCO_3$ particles and subsequent shear yielding of the matrix, intense crazing (or craze-like) and finally diffused crazing	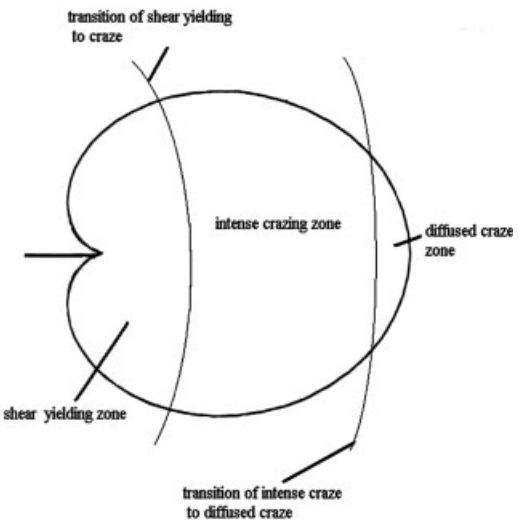

Figure 12 The sequences of fracture toughness micromechanisms in pure PP and PP/$CaCO_3$ nanocomposites.

CONCLUSIONS

Based on the results obtained, the following conclusions can be drawn:

- Nano $CaCO_3$ acts as a nucleating agent and destroys the spherulitic structure of the polypropylene matrix.

- It can be said that all PP/$CaCO_3$ nanocomposites have higher fracture toughness than that of pure PP. The J_c value increased up to approximately two times that of pure PP at 5 wt % of $CaCO_3$.
- In general, in PP/$CaCO_3$ nanocomposites, debonding of calcium carbonate triggers shear yielding of polypropylene matrix.
- The fracture micromechanisms varied from rubber particles cavitation and shear yielding in pure co-PP to simultaneous existence of rubber particles cavitation, filler particles debonding, shear yielding, and intense and diffused crazing in PP/$CaCO_3$ nanocomposites.

References

1. Platt, D. K. Engineering and High Performance Plastics Market Report; Rapra Technology: Europe, 2003.
2. Pukanszky, P. In Polypropylene, Structure, Blends and Composites; Karger-Kocsis, J., Ed.; Chapman & Hall: UK, 1995; Vol. 3, p 1.
3. McGenity, P. M.; Hooper, J. J.; Paynter, C. D.; Riley, A. M.; Nutbeem, C.; Elton, N. J.; Adams, J. M. Polymer 1992, 33, 5215.
4. Pukanszky, B.; Belina, K.; Rockaebauer, A.; Maurer, F. H. J. Composites 1994, 25, 205.
5. Karger-Kocsis, J. In Polypropylene, Structure, Blends and Composits; Karger-Kocsis, J., Ed.; Chapman & Hall: UK, 1995; Vol. 3, p 142.
6. Zebarjad, S. M.; Tahani, M.; Sajjadi, S. A. J. Mater Proc Tech 2004, 155/156, 1459.
7. Zebarjad, S. M.; Bagheri, R.; Lazzeri, A.; Serajzadeh, S. Mater Des 2004, 25, 247.
8. Starke, J. U.; Michler, G. H.; Grellmann, W.; Seidler, S.; Gahleitner, M.; Flebig, J.; Nezbedova, E. Polymer 1998, 39, 75.
9. Chan, C. M.; Wu, J.; Li, J. X.; Cheung, Y. K. Polymer 2002, 43, 2981.
10. Thio, Y. S.; Argon, A. S.; Cohen, R. E.; Weinberg, M. Polymer 2002, 43, 3661.
11. Golebiewski, J.; Galeski, A. Compos Sci Technol 2007, 67, 3442.
12. Zhang, M.; Liu, Y.; Zhang, X.; Gao, J.; Huang, F.; Song, Z.; Wei, G.; Qiao, J. Polymer 2002, 43, 5133.
13. Weon, J.-I.; Boo, W.-J.; Gam, K.-T.; Sue, H.-J.; Chan, C.-M. J Appl Polym Sci 2006, 99, 3070.
14. Avella, M.; Cosco, S.; Di Lorenzo, M. L.; Di Pace, E.; Errico, M. E.; Gentile, G. Eur Polym J 2006, 42, 1548.
15. Garcia-Lopez, D.; Merino, J. C.; Pastor, J. M. J Appl Polym Sci 2003, 88, 947.
16. Zokaei, S.; Lesan Khosh, R.; Bagheri, R. Mater Sci Eng A 2007, 445/446, 526.
17. Hanim, H.; Ahmad Fuad, M. Y.; Zarina, R.; Mohd Ishak, Z. A.; Hassan, H. J Thermoplast Compos Mater 2008, 21, 123.
18. Chen, J.; Wang, G.; Zeng, X.; Zhao, H.; Cao, D.; Yun, J.; Tan, C. K. J Appl Polym Sci 2004, 94, 796.
19. Yang, K.; Yang, Q.; Li, G.; Sun, Y.; Feng, D. Mater Lett 2006, 60, 805.
20. Zhang, Q.-X.; Yu, Z.-Z.; Xie, X.-L.; Mai, Y.-W. Polymer 2004, 45, 5985.
21. Hornsby, P. R.; Premphet, K. J Mater Sci 1997, 32, 4767.
22. Sue, H.-J.; Yee, A. F. J Mater Sci 1993, 28, 2975.
23. Karger-Kocsis, J. Poypropylene an A–Z Reference; Kluwer Academic Publishers: Dordrecht, 1999.
24. Zuiderduin, W. C. J.; Westzaan, C.; Huetink, J.; Gaymans, R. J Polym 2003, 44, 261.
25. Demjen, Z.; Pukanszky, B.; Nagy, J. Composites Part A 1998, 29, 323.
26. Kiss, A.; Fekete, E.; Pukanszky, B. Compos Sci Technol 2007, 67, 1574.
27. Wei, G.-X.; Sue, H.-J. Polym Eng Sci 2000, 40 1979.
28. Zebarjad, S. M.; Sajjadi, S. A.; Tahani, M. J Mater Proc Tech 2006, 175, 446.